

Circularly-polarized THz wave emission from a micro-thin water flow

Hsin-hui Huang

Academia Sinica

Saulius Juodkazis

Swinburne University of Technology <https://orcid.org/0000-0003-3897-2844>

Eugene Gamaly

Australian National University

Takeshi Nagashima

Setsunan University

Tetsu Yonezawa

Hokkaido University <https://orcid.org/0000-0001-7371-204X>

Koji Hatanaka (✉ kojihntnk@gate.sinica.edu.tw)

Academia Sinica

Article

Keywords: water-based THz emission, pulse irradiation, non-ionizing radiation

Posted Date: October 11th, 2021

DOI: <https://doi.org/10.21203/rs.3.rs-77877/v2>

License:   This work is licensed under a Creative Commons Attribution 4.0 International License.

[Read Full License](#)

Circularly-polarized THz wave emission from a micro-thin water flow

Hsin-hui Huang¹, Saulius Juodkazis^{2,3,4*}, Eugene G. Gamaly⁵, Takeshi
Nagashima^{6**}, Tetsu Yonezawa^{7,8}, and Koji Hatanaka^{1,9,10***}

¹Research Center for Applied Sciences, Academia Sinica, Taipei 11529, Taiwan

²Centre for Micro-Photonics and ARC Training Centre in Surface Engineering for Advanced
Materials (SEAM), School of Science, Swinburne University of Technology, Hawthorn, VIC
3122, Australia

³Tokyo Institute of Technology, 2-12-1 Ookayama, Meguro-ku, Tokyo 152-8550, Japan

⁴Institute of Advanced Sciences, Yokohama National University, 79-5 Tokiwadai,
Hodogaya-ku, Yokohama 240-8501, Japan

⁵Laser Physics Centre, Research School of Physics and Engineering, The Australian
National University, Canberra, ACT 0200, Australia

⁶Faculty of Science and Engineering, Setsunan University, 17-8 Ikeda-Nakamachi, Neyagawa,
Osaka 572-8508, Japan

⁷Division of Materials Science and Engineering, Faculty of Engineering, Hokkaido
University, Hokkaido 060-8628, Japan

⁸Institute for the Promotion of Business-Regional Collaboration, Hokkaido University,
Hokkaido 001-0021, Japan

⁹College of Engineering, Chang Gung University, Taoyuan 33302, Taiwan

¹⁰Department of Materials Science and Engineering, National Dong-Hwa University, Hualien
97401, Taiwan

Intense THz wave sources are highly expected for further progresses in nonlinear THz science and practical implementation of non-ionizing radiation in sensing and communications. Solid-based sources have inherent limits of material breakdown, while intense laser irradiation of liquids is a promising emerging technique for THz wave and hard X-ray emission. Water-based THz emission shows intensity enhancements up to 10^3 times when laser-pulse pairs with nanosecond delay are used. Here we show circularly-polarized THz wave emission from thin water flow irradiated by two time-separated and linearly-polarized femtosecond laser pulses. THz time-domain spectroscopy reveals the circularly-polarized THz emission dominates 4.7 ns after the first pulse irradiation. THz wave detection delay in the spectroscopy and time-resolved micrography indicate that the THz wave emission originates from the rarefied volume in front of the flow. Radial relaxation of charges in the focal volume where ponderomotive charge depletion occurred on the optical axis is the origin for the circular polarization (due to spiraling currents). Tight focusing of fs-laser pulses localized THz wave emission to the sub-wavelength (tens-of-micrometers) region.

42 Along with the fertile progresses in THz science and technology, intense and
 43 tunable THz wave radiation has been expected for advanced applications such
 44 as non-linear THz science [1]. Though there are various types of THz wave
 45 sources from electrically-driven devices to femtosecond laser methods based on
 46 optical rectification with nonlinear solid crystals and laser-plasma with targets
 47 of gases and clusters [2]. The solid targets have their own inherent limitations
 48 for the incident laser power because of the target irreversible damages, therefore
 49 scaling up intense THz wave radiation cannot be achieved. Since liquids such
 50 as water is a renewable target, it can be used under intense laser irradiation
 51 for THz emission [3–5] simultaneously with X-ray emission from hot plasma [5].
 52 Water has another characteristic as a universal polar solvent, which will expand
 53 the tunability of THz wave sources [6].

54 Furthermore, not only the THz intensity but its polarisation is important.
 55 Circularly-polarised THz sources are required in the study of laser filamenta-
 56 tion [7,8], spin dynamics of solid state materials [9], chirality of proteins [10]. In
 57 material sciences, the state of angular momentum of light, i.e., its polarisation,
 58 effects the optical excitation [11], spectroscopy [12–14], sensing and commu-
 59 nications [2], and provides data transfer multiplexing in information technolo-
 60 gies [15]. However, there is lack of low loss polarisation optical waveplates for
 61 THz spectral range, what makes generation methods of circularly polarised THz
 62 sought after.

63 There are reports of circularly-polarized THz wave emission from plasma
 64 under a two-color laser excitation [16–20]. The ellipticity of the THz wave
 65 can be controlled by the filament length with suitable input laser energy [21],
 66 the relative phase between the fundamental wave and the second harmonic
 67 pulses [22–24], the pulse energy [25], and changing the time delays between
 68 three-pulse configuration [26]. Polarisation of THz wave emission from the fila-
 69 ment of optically induced plasma was described by considering a dipole radiation
 70 inside ~ 1 mm water jets [27, 28] or in air [29] oriented along the propagation
 71 of femtosecond laser pulses and formed as a result of ponderomotive force. The
 72 ponderomotive force behind the ionisation front of a self-guided femtosecond
 73 laser pulse in air created a $L = 1 - 30$ cm long, ~ 0.1 mm diameter filaments
 74 which induced THz wave emission with a spatial intensity and polarisation pat-
 75 tern defined by a moving dipole mechanism [29]. The polarisation of THz wave
 76 emission was found to be linear-radial (in respect to the propagation axis) as
 77 revealed by the squared Malus dependence $\propto \sin^4 \theta$. In this study, we investi-
 78 gate the case when the filament length, L , is sub-wavelength (sub-1 mm) at the
 79 tight focusing when L corresponds to the geometrical focus, i.e., the Rayleigh
 80 length (see, the concept illustration in Fig. 1). Tight focusing of ultrashort laser
 81 pulses has additional benefit for the higher THz wave emission due to scaling
 82 for the ponderomotive force induced wake field dipoles, $P_{THz} = \frac{1}{7} \left(\frac{E_p}{w_0} \right)^2 \left(\frac{\lambda}{t_p} \right)^4$,
 83 where $w_0 = 0.61\lambda/NA$ is the waist of the laser beam at the focus (a lens with
 84 numerical aperture NA), t_p is pulse duration and λ is its wavelength [30]. THz
 85 wave emission from sub-wavelength filaments is not yet explored research area
 86 which is strongly required for ultimate control of intensity, direction, phase, and

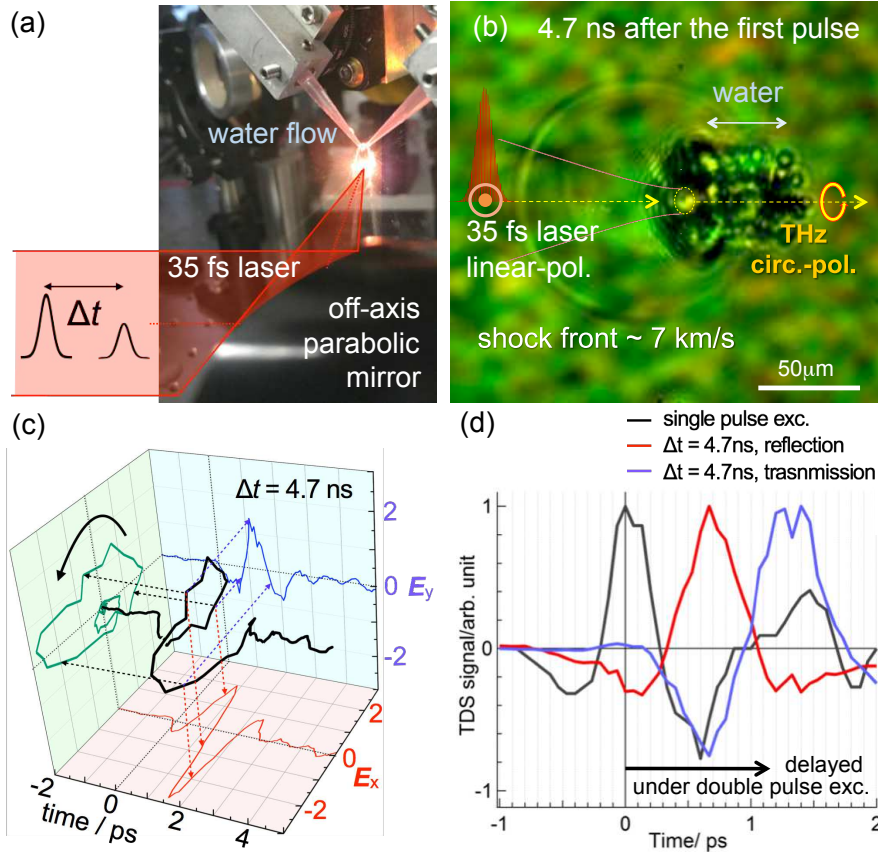


Figure 1: Concept: tailoring the light-matter interaction for the polarization manipulation of THz wave. (a) A thin water flow irradiated by a pair of femtosecond laser pulses (35fs, 800nm) for THz wave generation. Pulses are tightly focused to a $\sim 10 \mu\text{m}$ spot on the surface of a $17 \mu\text{m}$ -thick water flow. (b) Time-resolved shadowgraphy with $\sim 1 \text{ ps}$ temporal resolution; a representative photo captured at 4.7 ns after the first pulse irradiation. Details are in [Suppl. S1.2](#) and [Fig. S2](#). (c) Signals in THz time-domain spectroscopy (TDS) when the delay time at 4.7 ns, which indicates the circularly-polarized THz wave emission. Details are in [Suppl. S1.1](#) and [Fig. S1](#). (d) TDS time delay observed under the double pulse excitation; here TDS measurements were not polarization-discriminated.

87 polarisation of THz wave sources.

88 Creation of single-cycle THz wave sources and to control their polarisation
 89 could open a versatile toolbox of polarisation sensitive characterisation tech-
 90 niques currently developed at a rudimentary level. This study shows a promising
 91 direction towards generation of a single cycle circularly-polarised THz wave from
 92 focus of femtosecond laser pulse with sub-wavelength extension (for THz wave).
 93 Small sub-wavelength THz wave emitters provide flexibility in engineering THz

94 wave sources with complex wavefronts, polarisation, and high power currently
 95 achieved by millimeters-long filaments [31]. Here, we report circularly-polarized
 96 THz wave emission from micro-thin water flow under double-pulse cross-linearly-
 97 polarized laser excitation. Axial extension of the THz wave-emitting filament
 98 of the second pulse (the main pulse) is enclosed inside the expanding water
 99 plume created by the first pulse (the pre-pulse) and has approximately the
 100 length of focal region of $60 \mu\text{m}$ at the focusing conditions. The most efficient
 101 THz wave emission corresponded to the pulse separation of 4.5-5 ns. A cur-
 102 rent generated to restore charge depletion along the optical axis due to action
 103 of the ponderomotive force with simultaneously occurring recombination be-
 104 tween ions and electrons is 1-2 ps long defining the spectrum of THz wave
 105 emission. Detailed polarisation analyses of THz E -fields in the transmission
 106 and reflection directions are carried out by time-domain spectroscopy revealing
 107 peculiarities of sub-wavelength THz wave emission. The region of THz wave
 108 emission is also captured by time-resolved shadowgraphy/luminescence imaging
 109 experiments which confirm the origin of THz wave emission is in front, but not
 110 inside, of the water flow (Fig. 1).

111 Results

112 **Circularly-polarised THz wave emission.** Figure 1(c) shows polarisation
 113 resolved emission of THz wave at the optimum conditions with delay between
 114 two pulses of 4.7 ns using time-domain spectroscopy (TDS); more details are
 115 described in Suppl. S1.1 with Fig. S1 where the E_x and E_y are measured in
 116 the transmission and the reflection directions. THz wave emission under the
 117 single pulse excitation maintains the same E_x polarization with the main pulse.
 118 However, under the double pulse excitation, THz wave emission changes its
 119 polarization from linear to circular as the delay time advances and its intensity
 120 reaches the highest at the delay time of 4.7 ns as reported previously without
 121 detailed polarisation analysis [32]. THz wave emission spectra obtained from
 122 TDS signals by discrete Fourier-transform, as shown in the inset in Fig. S1,
 123 show their peak shifts toward the lower frequency as the delay time increases.
 124 This indicates that the the interaction length of the main pulse E_2 with the
 125 ablated water plume after the pre-pulse E_1 irradiation becomes longer.

126 **Direct imaging of light-water interaction.** Figure 1(b) shows the time-
 127 resolved shadowgraphy image captured by back-side illumination of picosecond
 128 white light continuum at the maximum enhancement of THz wave emission.
 129 It clearly defines the geometry of the focal spot which is important in the es-
 130 timation of light-matter conditions in the case on THz wave emission. The
 131 focus diameter on the flow was close to the geometrical focus with the radius
 132 $\sim 0.61\lambda_l/NA \approx 4 \mu\text{m}$; $NA = 0.125$ is the effective numerical aperture of the
 133 off-axis parabolic mirror. This is markedly different from THz wave emission in
 134 self-guided filament formation in air ($\sim 100 \mu\text{m}$ diameter and centimeters-long)
 135 governed by self-focusing of femtosecond laser pulses [29]. Detailed evolution

136 of micro-explosion is presented in details in shadowgraphs (Fig. S2 in Suppl.
 137 S1.2) revealing the evolution of the shockwave induced by the pre-pulse irradiation.
 138 Shockwave expansion velocity in air was approaching 7.6 km/s, which
 139 corresponds to strong explosion conditions. The radius of the shocked hemi-
 140 sphere in front of the water flow is $R \approx 60 \mu\text{m}$ (at the delay time of 4.7 ns)
 141 when the diameter of laser on the water is $w_0 \approx 8 \mu\text{m}$ and depth of ablation is
 142 $h \approx 2 \mu\text{m}$. The additional ablated volume of water constitutes only 0.02% of
 143 volume in the shocked region, however, the molecular number density of water
 144 is 1.237×10^3 larger as compared with air. As a result, the molecular density
 145 of the water-air is at least by 26% larger as it is for the first pulse. This allows
 146 the plasma to reach higher density by the second pulse E_2 . Indeed, as shown in
 147 the luminescence images (Fig. S2 in Suppl. S1.2), interaction of the main pulse
 148 with water flow previously modified by the pre-pulse irradiation becomes more
 149 dominant. The very central part of light-matter interaction on the flow surface
 150 is the source of X-ray emission since the electron temperature reaching $\sim 1 \text{ keV}$
 151 is achieved under the experimental conditions [5, 32] (see Suppl. S1.3; however,
 152 this study was solely focused on THz wave emission).

153 Figure 1(d) shows the time delay in TDS signals observed at the different
 154 excitation conditions. The TDS signals under the double pulse excitation delay
 155 for $\sim 700 \text{ fs}$ in the reflection and for $\sim 1.4 \text{ ps}$ in the transmission. By considering
 156 that the refractive index of water at 1 THz is ~ 2.12 [33], it is consistent with
 157 direct imaging and indicates that the conversion from the near-IR laser to THz
 158 wave takes place in front of the original water flow surface. This observation
 159 indicates that the ablation of water by the pre-pulse E_1 and the shockwave
 160 dynamics is important for the THz wave emission under the double pulse excitation.
 161 The location of THz wave emission is presented earlier to originate
 162 from the inside of water flow [34] which is in this case highly unlikely due to
 163 extraordinary-high plasma density (water molecular density $3.35 \times 10^{22} \text{ cm}^{-3}$)
 164 for the ponderomotive mechanism under employed intensity range.

165 **Radial charge transport at the tight focus.** Figure 2 shows the key fea-
 166 tures on the light-matter interaction relevant for the circularly-polarised THz
 167 wave emission. The second/main pulse E_2 ionises the outwardly fast expanding
 168 gas and the water vapor generated by the pre-pulse E_1 . The most intense THz
 169 wave emission is observed at $\Delta t = 4.7 \text{ ns}$. This corresponds to the fast ($\sim 1 \text{ ps}$)
 170 currents along the optical path of the main pulse E_2 , which are due to electrons
 171 and ions radially depleted along the propagation due to the ponderomotive force
 172 which for electron is $F_p = -\frac{e^2}{4m_e\omega^2}\nabla I$, where I is the laser intensity. The ra-
 173 dial profile of the electronic density depletion on the axis of a Gaussian pulse
 174 $I(r) = I_0 e^{-4 \ln 2 (r/r_0)^2}$ is given by $N_e(r)/N_0 = 1 + \left(\frac{d^2}{dr^2} + \frac{1}{r} \frac{d}{dr}\right) \sqrt{1 + I^2(r)}$
 175 where $N_{e,0}$ is the electron and background densities, respectively, r_0 is the
 176 FWHM of the focal spot. The radial electron displacement has a steeper gradi-
 177 ent as compared with the axial charge separation due to ponderomotive force due
 178 to Gaussian intensity envelope. This is the key difference from the self-guided
 179 long filaments which never produced circularly-polarised THz wave emission

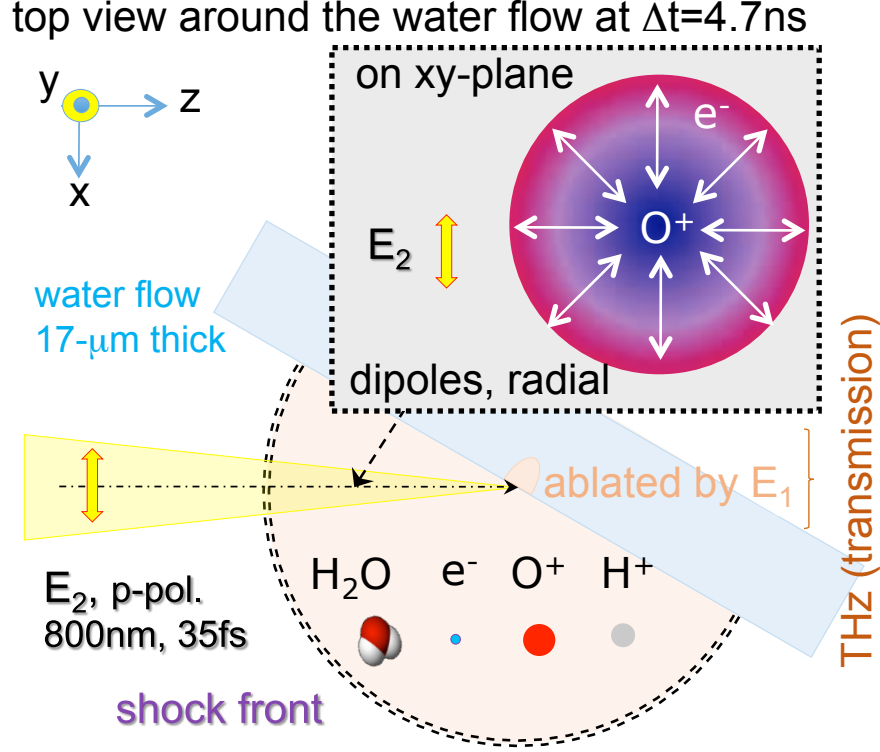


Figure 2: Geometry of the experiment for the $NA = 0.125$ focusing depicted after the pre-pulse E_1 (y-pol.) irradiation to the water flow which creates the expanding plasma region out of the ablated water flow (strong explosion with shockwave of radius r_{sh} ; see [Suppl. S1.2](#)). THz wave emission is induced by the current of ionised plasma rarefied along the center axis of the propagating E_2 laser pulse due to the radial ponderomotive force. The transient radial current $\partial J/\partial t$ is the source of THz wave emission. The Rayleigh length under the focusing conditions is $z_R \approx 60 \mu\text{m}$ ($2z_R$ is the depth-of-focus at 0.5-intensity level, i.e. FWHM), which would correspond to the $\lambda_{THz}/4$ for the emission at 1.25 THz ($240 \mu\text{m}$).

180 since the radiating dipole (via Cherenkov-like mechanism) is axially oriented.
 181 The radial pattern of arrows in the xy-plane cross-section shows charge separation
 182 by the ponderomotive force (the radial pattern will occur for electrons,
 183 protons H^+ and O^+ which will have different radial distribution due to their
 184 difference in mass; see [Suppl. S1.3](#)). The radial ion-electron charge diffusion
 185 and recombination onto the optical axis takes place in the wake of the optical
 186 pulse. This ultrafast current transient is the source of THz wave emission which
 187 is phase-tailored into circularly-polarised radiation as the second pulse (35 fs
 188 or $10 \mu\text{m}$) ionised the $\sim 60 \mu\text{m}$ long focal region. The current was initiated
 189 at the locations further away from the focus and propagated towards the water

190 flow. It was shown that the circularly spiraling current will generate circularly-
191 polarised THz radiation when spiral electrodes were used [35]. Previous studies
192 with linearly-polarised light pulses have shown that in the case of irradiation
193 of Ar cluster in vacuum by two time-separated pulses, the polarisation of the
194 THz wave emission was defined along the line through the center of the first
195 pulse and the position of the focus of the second pulse (which was shifted out
196 of center by $\sim 40 \mu\text{m}$) [36]. The intensity of the first pulse was inducing the
197 charge depletion on the axis with positive ions closer to the center (on the op-
198 tical axis). Electrons generated out-off-the-center by the second pulse caused
199 a linear current (towards the center) and consequently linearly-polarised THz
200 wave emission. The conditions of tight focusing explored in our study creates
201 spatially confined plasma at the focal region along the optical axis. Since elec-
202 trons, protons, and oxygen ions from the water flow (and oxygen and nitrogen
203 from air) are separated radially to the different position by the pre-pulse, the
204 second pulse initiates a spiraling current along the depth-of-focus (more details
205 are discussed in [Suppl. S1.4](#)). The irradiation position of the first pulse to that
206 of the main pulse is optimised for the strongest THz wave emission by the same
207 methodology as we described earlier for the maximum of X-ray emission [32];
208 i.e., slight walk-off on the xy-plane is introduced for the maximum of the emis-
209 sion. This optimisation is obtained for approximately $10 \mu\text{m}$ shift along the
210 x-axis on the flow surface. Quantification of the offset from the optical axis
211 for the intensity and polarisation control of THz wave emission needs further
212 studies. It is established in this study that the circularly-polarised single cycle
213 THz pulse can be generated using the tight optical-focusing from ionised focal
214 volume in the pre-plasma with the axial extent of $\lambda/4$ of THz wave emission.

215 Conclusions

216 A simple two-laser pulse irradiation to a thin water flow is shown to generate
217 circularly-polarized THz wave emission from a plasma filament which has length
218 of approximately quarter wavelength of the THz emission (a sub-wavelength
219 THz emitter). The mechanism responsible for the increased efficiency of THz
220 wave emission as compared with the single pulse irradiation of solid/liquid/gas
221 targets is related to water ablation inside strong shock region in air in front of
222 the water flow. The ablation condition for THz wave emission is optimal at the
223 delay time 4.7 ns after the pre-pulse irradiation. The radial current transients
224 restoring axially depleted charges due to action of ponderomotive force deter-
225 mines the spectral extent (a shorter transient broader spectrum as related via
226 Fourier transform) and the circular polarisation of such THz wave emission. Cir-
227 cular polarisation is a result of radially spiraling currents which originate along
228 the $\lambda_{THz}/4$ long Rayleigh region of optical focus (a linearly-polarised THz wave
229 are observed from the axially oriented dipole in self-guided long filaments [29]).
230 THz wave emission in the reflection and transmission directions in respect to the
231 water flow has similar intensities but opposite polarisation. The transmission
232 losses of sub-mm wavelength THz through $17\text{-}\mu\text{m}$ -thick water flow are slightly

233 reducing the transmitted power. As previously reported [32], the highest inten-
234 sity of THz wave emission from the water flow under the double pulse excitation
235 is 10-times higher in $|\mathbf{E}|^2$ (as photon numbers) than that from a $\langle 110 \rangle$ -oriented
236 ZnTe crystal. Further enhancements are expected in other liquids such as gold
237 nano-colloidal aqueous suspensions.

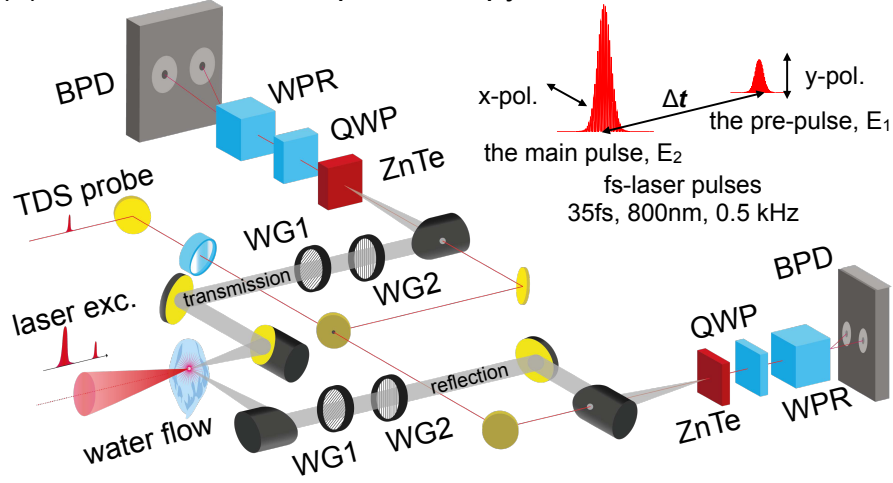
238 Circularly-polarised THz wave emission is adding new possibilities in a po-
239 larisation control toolbox for THz technologies which can open new applications
240 for opto-mechanics where large torsion can be generated upon absorption, reflec-
241 tion, or scattering and for rotational/vibrational molecular spectroscopy where
242 polarisation wave-plates are not readily available or lossy. THz wave can be
243 used to better understand highly dynamic laser triggered explosions which find
244 increasing number of application in laser machining/fabrication and creation of
245 high temperature/pressure phases of new materials. Among different methods
246 of electromagnetic field generation, sub-wavelength emitters are promising due
247 to unmatched flexibility in wave front and polarisation engineering.

248 Methods

249 All the experiments shown in Fig.3 were carried out in air under atmospheric
250 pressure (1 atm) at room temperature (296 K).

251 **Polarization-sensitive THz time-domain spectroscopy.** A pulsed fem-
252 tosecond laser ($t_p = 35$ fs, transform-limited, $\lambda = 800$ nm, 1 kHz, Mantis,
253 Legend Elite HE USP, Coherent, Inc.) is used and the output pulses are split
254 into the pre-pulse (E_1 , linearly-polarized parallel to y-axis, y-pol., 0.1 or 0.2
255 mJ/pulse), the main pulse (E_2 , linearly-polarized parallel to x-axis, x-pol., 0.4
256 mJ/pulse), and the probe for THz time-domain spectroscopy (TDS) with a
257 series of half-wave plates and polarization beam splitters (65-906, 47-048, Ed-
258 mund Optics) as shown in Fig. 2 (a) [5, 6, 32]. THz wave emission is induced
259 by the irradiation of the co-linearly combined pre-pulse and main pulse onto a
260 thin water flow (~ 17 μm thick) by an off-axis parabolic mirror (1-inch diam-
261 eter, effective focal length $f = 50.8$ mm, 47-097, Edmund Optics). The laser
262 incident angle along z-axis is at 60° to the water surface normal. Under this
263 condition, the polarisations of the main and the pre-pulses are p-pol. and s-pol.,
264 respectively. The optical delay between the two excitation pulses, Δt , is con-
265 trolled with automatic stages (SGSP46-800 and SGSP26-150, Sigma Koki). A
266 water flow is prepared with two colliding water jets and the system is set on an
267 automatic stage (KS701-20LMS, Suruga Seiki) along the z-axis to adjust the
268 flow surface for optimal X-ray emission measured by a Geiger counter (SS315,
269 Southern Scientific). The detection of the THz wave emission is carried out by
270 the electro-optic sampling method in the transmission direction through the wa-
271 ter flow and in the reflection direction with $\langle 110 \rangle$ -oriented ZnTe crystals (1-mm
272 thick, Nippon Mining & Metals Co., Ltd.). Lock-in measurements are carried
273 out with an optical chopper (3502, New Focus) and a lock-in amplifier (SR830,
274 Stanford Research System), therefore the effective repetition rate of the laser
275 excitation is 0.5 kHz. Following the usual method reported previously [37–39],

(a) THz time-domain spectroscopy



(b) imagings

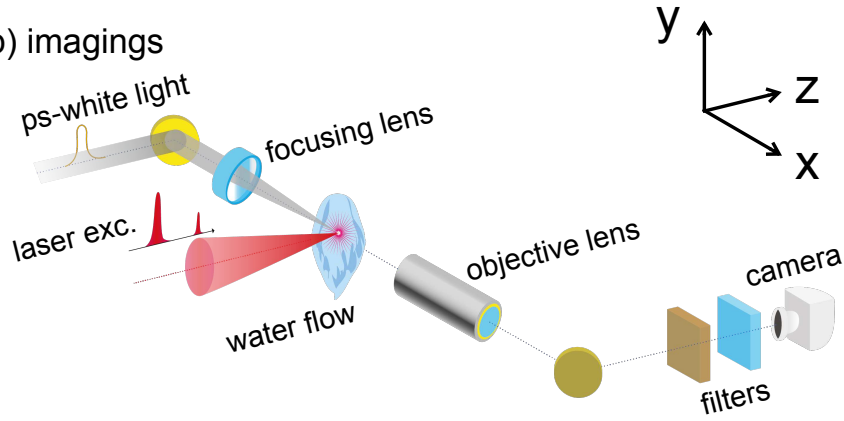


Figure 3: Schematic diagrams of the experimental setups with the water flow (17 μm thick) under the tight focusing of double pulses with the pre-pulse (x-pol., E_1) and the main pulse (y-pol., E_2) (a) for THz time-domain spectroscopy (TDS) with a ZnTe crystal (for electro-optic sampling) and (b) for time-resolved shadowgraphy and luminescence imaging. Δt indicates the delay time between the two pulses. Polarization statuses of THz wave emission were measured with a pair of wire-grids. Imaging experiments for the laser focus were also carried out with an objective lens and a color camera with the exposure time at 2 ms for the single shot. The details are in the text. QWP:quarter wave-plate, WPR:Wollaston prism, BPD:balanced photo-diode

276 two wire grids (WGs, MWG40FA-III, Origin) are additionally used for the mea-
 277 surements of polarization status in THz wave emission. One of the WGs, WG2,
 278 is used at the fixed angle 0° (parallel to x-axis), while the other WG, WG1, is
 279 used at two different angles, $+45^\circ$ and -45° for two independent TDS signals as
 280 E_{+45} and E_{-45} , respectively. The x- and y-components of THz electric field, E_x

281 and E_y , are then calculated from $E_x = E_{+45} + E_{-45}$ and $E_y = E_{+45} - E_{-45}$,
282 respectively.

283 **Time-resolved imagings.** Imaging experiments for the laser focus from the
284 side (along x-axis) are also carried out in two different methods with an objec-
285 tive lens (M Plan Apo 10 \times , MITUTOYO) and a color CMOS camera (Blackfly
286 S USB3, FLIR Systems, Inc.) with filters for IR-cut and for intensity control in
287 the visible region. One is with the pre-pulse and white light continuum (~ 1 ps,
288 580 ± 30 nm, as a strobe light) converted from the main pulse with a water
289 cell. With this method, transient refractive index changes and/or scattering
290 due to pre-plasma formation and/or laser ablation induced by the pre-pulse
291 irradiation can be visualized. Another imaging is with the pre-pulse and the
292 main pulse, which visualizes the interaction of the main pulse with the water
293 flow with structures prepared by the pre-pulse irradiation. The exposure time
294 for the camera setting was fixed at 2 ms for single shot imaging. In this mode
295 of image acquisition, all the emission in broad-band spectra by the two-pulse
296 irradiation of the water flow is time-integrated.

297 References

- 298 [1] K. Tanaka, H. Hirori, M. Nagai, IEEE Transactions on Terahertz Science
299 and Technology **2011**, 1, 1 301.
- 300 [2] J. A. Fülöp, S. Tzortzakis, T. Kampfrath, Advanced Optical Materials
301 **2020**, 8, 3 1900681.
- 302 [3] I. Dey, K. Jana, V. Y. Fedorov, A. D. Koulouklidis, A. Mondal, M. Shaikh,
303 D. Sarkar, A. D. Lad, S. Tzortzakis, A. Couairon, G. R. Kumar, Nat.
304 Commun. **2017**, 8, 1 1184.
- 305 [4] J. Qi, E. Yiwen, K. Williams, J. Dai, X.-C.Zhang, Appl. Phys. Lett. **2017**,
306 111, 7 071103.
- 307 [5] H.-H. Huang, T. Nagashima, W.-H. Hsu, S. Juodkazis, K. Hatanaka,
308 Nanomaterials **2018**, 8, 7 523.
- 309 [6] H.-H. Huang, Y.-t. R. Chau, T. Yonezawa, M. T. Nguyen, S. Zhu, D. Deng,
310 T. Nagashima, K. Hatanaka, Chemistry Letters **2020**, 49, 6 597.
- 311 [7] L. Bergé, S. Skupin, C. Köhler, I. Babushkin, J. Herrmann, Phys. Rev.
312 Lett. **2013**, 110 073901.
- 313 [8] L. Bergé, J. Rolle, C. Köhler, Phys. Rev. A **2013**, 88 023816.
- 314 [9] A. S. Prokhorov, V. B. Anzin, D. A. Vitukhnovskii, E. S. Zhukova, I. E.
315 Spektor, B. P. Gorshunov, S. Vongtragool, M. B. S. Hesselberth, J. Aarts,
316 G. J. Nieuwenhuys, M. Dumm, D. Faltermeier, S. Kaiser, S. Yasin, M. Dres-
317 sel, N. Drichko, Journal of Experimental and Theoretical Physics **2006**,
318 103, 6 887.

- 319 [10] X. Yang, X. Zhao, K. Yang, Y. Liu, Y. Liu, W. Fu, Y. Luo, Trends
320 Biotechnol. **2016**, 34 810.
- 321 [11] T. L. Cocker, V. Jelic, M. Gupta, S. J. Molesky, J. A. J. Burgess, G. D. L.
322 Reyes, L. V. Titova, Y. Y. Tsui, M. R. Freeman, F. A. Hegmann, Nature
323 Photonics **2013**, 7, 8 620.
- 324 [12] J. Zhu, Z. Ma, W. Sun, F. Ding, Q. He, L. Zhou, Y. Ma, Applied Physics
325 Letters **2014**, 105, 2 021102.
- 326 [13] B.-X. Wang, L.-L. Wang, G.-Z. Wang, W.-Q. Huang, X.-F. Li, X. Zhai,
327 Applied Physics A **2014**, 115, 4 1187.
- 328 [14] R. Singh, E. Plum, C. Menzel, C. Rockstuhl, A. K. Azad, R. A. Cheville,
329 F. Lederer, W. Zhang, N. I. Zheludev, Phys. Rev. B **2009**, 80 153104.
- 330 [15] S. Baierl, M. Hohenleutner, T. Kampfrath, A. K. Zvezdin, A. V. Kimel,
331 R. Huber, R. V. Mikhaylovskiy, Nature Photonics **2016**, 10, 11 715.
- 332 [16] D. J. Cook, R. M. Hochstrasser, Opt. Lett. **2000**, 25, 16 1210.
- 333 [17] M. Kress, T. Löffler, S. Eden, M. Thomson, H. G. Roskos, Opt. Lett. **2004**,
334 29, 10 1120.
- 335 [18] H. Zhong, N. Karpowicz, X.-C. Zhang, Applied Physics Letters **2006**, 88,
336 26 261103.
- 337 [19] I. Babushkin, W. Kuehn, C. Köhler, S. Skupin, L. Bergé, K. Reimann,
338 M. Woerner, J. Herrmann, T. Elsaesser, Phys. Rev. Lett. **2010**, 105 053903.
- 339 [20] Z. Zhang, N. Panov, V. Andreeva, Z. Zhang, A. Slepko, D. Shipilo, M. D.
340 Thomson, T.-J. Wang, I. Babushkin, A. Demircan, U. Morgner, Y. Chen,
341 O. Kosareva, A. Savel'ev, Applied Physics Letters **2018**, 113, 24 241103.
- 342 [21] Z. Zhang, Y. Chen, S. Cui, F. He, M. Chen, Z. Zhang, J. Yu, L. Chen,
343 Z. Sheng, J. Zhang, Nature Photonics **2018**, 12, 9 554.
- 344 [22] H. Wen, A. M. Lindenberg, Phys. Rev. Lett. **2009**, 103 023902.
- 345 [23] J. Dai, N. Karpowicz, X.-C. Zhang, Phys. Rev. Lett. **2009**, 103 023001.
- 346 [24] Y. S. You, T. I. Oh, K.-Y. Kim, Opt. Lett. **2013**, 38, 7 1034.
- 347 [25] Y. Chen, C. Marceau, S. Génier, F. Théberge, M. Châteauneuf, J. Dubois,
348 S. L. Chin, Optics Communications **2009**, 282, 21 4283 .
- 349 [26] H. Wang, N. Li, Y. Bai, P. Liu, Z. Wang, C. Liu, Opt. Express **2017**, 25,
350 25 30987.
- 351 [27] X.-C. Zhang, F. Buccheri, Lith. J. Phys. **2018**, 58, 1 1.

- 352 [28] E. Yiwen, Q. Jin, A. Tcypkin, X.-C. Zhang, Appl. Phys. Lett. **2018**, 113
353 181103.
- 354 [29] C. D’Amico, A. Houard, M. Franco, B. Prade, , A. Mysyrowicz, A. Coua-
355 iron, V. T. Tikhonchuk, Phys. Phys. Lett. **2007**, 98 235002.
- 356 [30] H. Hamster, A. Sullivan, S. Gordon, R. W. Falcone, Phys. Rev. E **2007**,
357 98 235002.
- 358 [31] A. Koulouklidis, C. Gollner, V. Shumakova, V. Fedorov, A. Pugžlys,
359 A. Baltuška, S. Tzortzakis, Nature Commun. **2020**, 11, 1 1.
- 360 [32] H.-H. Huang, T. Nagashima, T. Yonezawa, Y. Matsuo, S. H. Ng, S. Juod-
361 kazis, K. Hatanaka, Applied Sciences **2020**, 10, 6 2031.
- 362 [33] J. Zhou, X. Rao, X. Liu, T. Li, L. Zhou, Y. Zheng, Z. Zhu, AIP Advances
363 **2019**, 9, 3 035346.
- 364 [34] Q. Jin, J. Dai, E. Yiwen, X.-C. Zhang, Appl. Phys. Lett. **2018**, 113 261101.
- 365 [35] X. Lu, X.-C. Zhang, Phys. Rev. Lett. **2012**, 108 123903.
- 366 [36] K. Mori, M. Hashida, T. Nagashima, D. Li, K. Teramoto, Y. Nakamiya,
367 S. Inoue, S. Sakabe, Applied Physics Letters **2017**, 111, 24 241107.
- 368 [37] P. Yeh, Optics Communications **1978**, 26, 3 289 .
- 369 [38] F. Miyamaru, T. Kondo, T. Nagashima, M. Hangyo, Applied Physics
370 Letters **2003**, 82, 16 2568.
- 371 [39] N. Kanda, K. Konishi, M. Kuwata-Gonokami, Opt. Express **2007**, 15, 18
372 11117.

373 Acknowledgments

374 S.J. is grateful for partial support by the ARC Discovery DP190103284, Linkage
375 LP190100505 and JST CREST JPMJCR19I3 grants. T.N. is grateful for the sup-
376 port by JSPS KAKENHI Grant Number 20K05371. T.Y. is grateful for the support
377 by Grant-in-Aid for Scientific Research for Fostering Joint International Research (B)
378 (18KK0159). K. H. is grateful for the supports by the Ministry of Science and Technol-
379 ogy (MOST) of Taiwan (107-2112-M-001-014-MY3), the Cooperative Research Pro-
380 gram of “Network Joint Research Center for Materials and Devices“, Nanotechnology
381 Platform (Hokkaido University), and the Collaborative Research Projects of Labora-
382 tory for Materials and Structures, Institute of Innovative Research (Tokyo Institute
383 of Technology). K. H. also acknowledges the Japan Science and Technology Agency
384 (JST) PRESTO (Precursory Research for Embryonic Science and Technology) Pro-
385 gram (SAKIGAKE, Innovative use of light and materials/life) for its supports on the
386 original project on X-ray/THz wave simultaneous emission, ”Ultrawide band light
387 conversion by controlling structures of microdroplets and ultrashort laser pulse (2009-
388 2013)” and for the laser facilities for the current project. H. -H. H. and K. H. acknowl-
389 edge Mr. Yung-Jie Huang for his drawings of the experimental setups.

Supplementary Files

This is a list of supplementary files associated with this preprint. Click to download.

- [THzPolNatCommsupplement.pdf](#)